Joule

CellPress

Article

Gigantic triboelectric power generation overcoming acoustic energy barrier using metal-liquid coupling

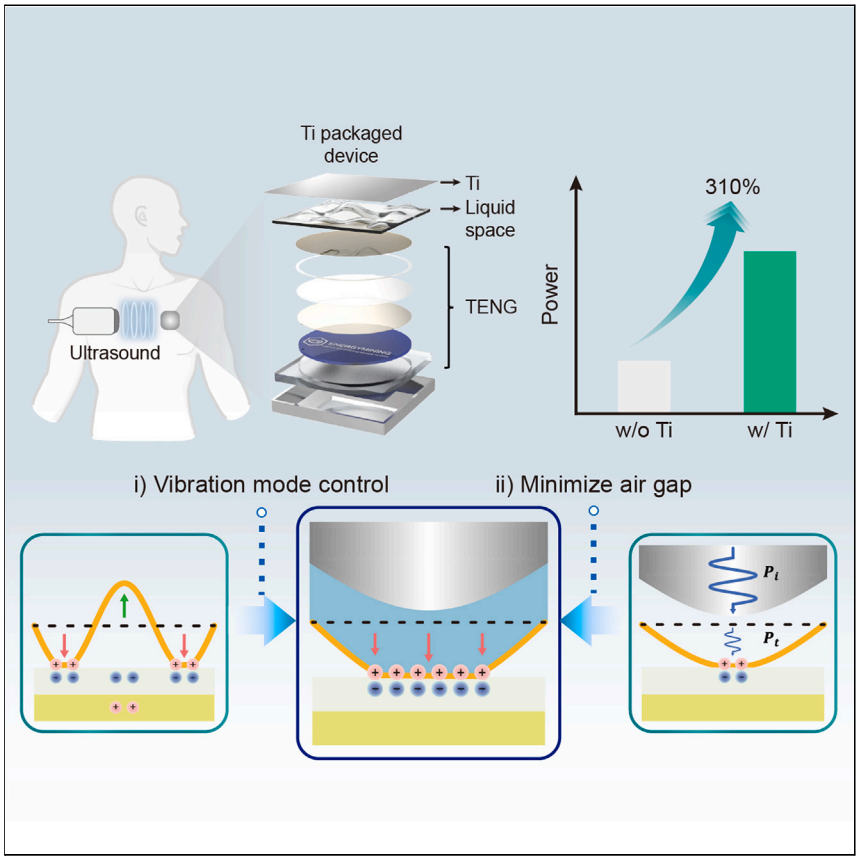

Titanium packaging in implantable medical devices (IMDs) plays the contradictory role of protecting internal components while impeding energy transfer. Our work provides a wireless energy transfer technology that can overcome the energy attenuation caused by the packaging. Our strategy exploits the elastic wave generated in a titanium layer by an ultrasound source. This method induces unimodal vibrations in a triboelectric membrane, significantly increasing the efficiency. We expect this technology to pave the way for the next generation of IMDs.

Youngwook Chung, Jang-Mook Jeong, Joon-Ha Hwang, ..., Hyun-moon Park, Hong-Joon Yoon, Sang-Woo Kim

kimagu@energymining.co.kr (H.-m.P.)
yoonhj1222@gachon.ac.kr (H.-J.Y.)
kimsw1@yonsei.ac.kr (S.-W.K.)

Highlights

Ultrasound is attenuated by titanium packaging but still transmits vibrations

The unidirectional vibration of titanium can be transmitted via a liquid medium

The output power of TENG is amplified through the vibration mode control

The miniaturized titanium-packaged device enables Bluetooth communication

Chung et al., Joule *8*, 1–15
September 18, 2024 © 2024 Elsevier Inc. All rights are reserved, including those for text and data mining, AI training, and similar technologies.
https://doi.org/10.1016/j.joule.2024.06.016

Please cite this article in press as: Chung et al., Gigantic triboelectric power generation overcoming acoustic energy barrier using metal-liquid coupling, Joule (2024), https://doi.org/10.1016/j.joule.2024.06.016

Joule

CellPress

Article

Gigantic triboelectric power generation overcoming acoustic energy barrier using metal-liquid coupling

Youngwook Chung,[1,2,10] Jang-Mook Jeong,[1,2,10] Joon-Ha Hwang,[1,2,10] Young-Jun Kim,[2] Byung-Joon Park,[3,4] Daniel S. Cho,[2] Youngmin Cho,[1] Su-Jeong Suh,[2] Byung-Ok Choi,[5,6,7] Hyun-moon Park,[1,*] Hong-Joon Yoon,[8,9,*] and Sang-Woo Kim[1,3,4,11,*]

SUMMARY

Hermetically sealed titanium (Ti) packaging provides protection for implantable medical devices, but it hinders reliable wireless power transfer to these devices. We present a miniaturized device that utilizes ultrasound-induced vibrations in Ti, mediated by liquid space, for efficient triboelectric energy harvesting. Unlike the conventional ultrasound-driven triboelectric nanogenerator, which induces contact electrification through multiple modes, the Ti-packaged device generates vibrations of the triboelectric membrane in a single mode, facilitating effective energy transfer. The incorporation of the Ti packaging leads to a significant increase in power density, up to 310% compared with the absence of it when measured under a tissue-mimicking material, and it enables long-term stability and Bluetooth communication *in vivo*. These findings represent the first technology that enhances power transmission characteristics through a Ti layer. We believe that this technology will accelerate the development of smaller, multifunctional, and long-lasting implantable medical devices.

INTRODUCTION

Transcutaneous energy transfer (TET) systems are vital in the modern medical field, where millions of implantable medical devices (IMDs) fulfill the desire to increase human longevity by being isolated inside the body.[1–4] A recent report introduced an ultrasound-driven vibrating triboelectric nanogenerator (US-TENG) that harvests ultrasound, commonly utilized in medical fields, and the triboelectrification phenomenon induced by vibrations of a membrane.[5] This technology has demonstrated its potential for TET systems in various biomedical applications, such as recharging batteries for IMDs, wound healing, and treating neuropathy.[5–9] The practical use of US-TENGs in commercial IMDs requires a power generation module that can reliably provide power[10,11] while being embedded within packaging that ensures not only biocompatibility but also long-term hermetic sealing of internal components against body fluids.[12,13] In this regard, titanium (Ti) and its alloys have remained the standard packaging materials for commercial IMDs for decades.[14] Despite its advantages of stability, Ti packaging poses a significant challenge for energy transfer. For instance, radio frequency electromagnetic waves are shielded by Ti packaging, necessitating complex packaging methods,[15] including polymeric materials.[16,17] Ultrasound waves also encounter significant energy reflection and a sharp decrease in transmission through the packaging due to the acoustic impedance of Ti being over 20 times

CONTEXT & SCALE

Implantable medical devices are crucial for human health but struggle with energy sourcing due to their prolonged implantation within the human body. An ultrasound-driven triboelectric nanogenerator based on the contact-electrification phenomenon is a safe and promising energy solution for such devices. The challenge, however, lies in the titanium (Ti) packaging of implantable medical devices. Although this packaging ensures mechanical stability and biocompatibility, it hinders efficient energy transfer.

In this work, we introduce a new approach, increasing power density by up to 310% via a Ti layer combined with a liquid space. This strategy addresses two primary challenges: efficiently harnessing acoustic energy to overcome the energy barrier and controlling the vibration mode for effective energy harvesting. We anticipate that this research will pave the way for the development of smaller, more functional implantable medical devices with extended lifetimes.

All rights are reserved, including those for text and data mining, AI training, and similar technologies.

Please cite this article in press as: Chung et al., Gigantic triboelectric power generation overcoming acoustic energy barrier using metal-liquid coupling, Joule (2024), https://doi.org/10.1016/j.joule.2024.06.016

that of soft tissue.[18] Recent research implemented an acoustic energy transfer system using a US-TENG to operate a pulse generation circuit through a Ti-packaged IMD.[19] However, the application of the Ti packaging resulted in a significant reduction in power output, which impedes its versatile functionality.

To achieve efficient energy transfer through Ti packaging, it is essential to design US-TENGs capable of amplifying acoustic energy or generating power efficiently from a given acoustic energy. Research has been reported on utilizing metamaterials such as phononic crystals and locally resonant acoustic metamaterials to modulate and amplify mechanical waves for effective energy harvesting.[20,21] Despite the potential of this research, the application of modulated ultrasound energy to energy harvesting is still in its early stages, and the complicated structure and bulky dimensions of metamaterials hinder its application to IMDs. Furthermore, it is important to take into account the vibration characteristics of the triboelectric membrane. This is essential as the electrical potential change induced by membrane vibration determines the current output of US-TENGs. In previous studies, ultrasound irradiation has induced multiple vibration modes of the membrane that move simultaneously in the up and down directions, causing an offset in the induced electrical potential.[5] While a micro-electro-mechanical system (MEMS)-based resonant configuration has been proposed to enhance the displacement of a membrane, its utilization of silicon as the vibrating membrane led to suboptimal power output.[22] A rational design of the vibrating membrane for harvesting ultrasound energy has been proposed through computational analysis, but its practical implementation is yet to be realized.[23]

Herein, we introduce a novel strategy to enhance the power density of US-TENGs by up to 310% through Ti packaging coupled with a liquid space, as compared with the non-packaged device. This enhancement is achieved by addressing the two aforementioned challenges: efficiently harvesting the provided acoustic energy and achieving control over the vibration mode of the membrane. Our method harnesses the elastic wave generated in the Ti plate by an ultrasound source. As ultrasound waves pass through the Ti plate, the plate exhibits a vibrational behavior closer to a single mode rather than a multimode vibration. By removing the entrapped air pockets, the liquid space can effectively transmit elastic waves from the Ti plate to the triboelectric membrane, thereby modulating the membrane's vibration mode. Notably, the power density of the device integrating liquid with the Ti packaging surpasses its non-liquid counterpart by a factor of 64. Using the strategy, we implemented a miniaturized, Ti-vibrating, and implantable TENG (TI-TENG) and demonstrated its powerful energy transfer performance through tissue-mimicking material (TMM) and *in vivo* environments. The results highlight the great potential of the strategy for effective energy transfer through Ti packaging and confirm its applicability to IMDs with smaller dimensions and more functionality.

RESULTS

Design and working principle of the TI-TENG

A miniaturized, fully Ti-packaged TI-TENG is designed to efficiently harvest ultrasound energy based on the triboelectric phenomenon (Figure 1A). The inset in Figure 1A displays a photograph of the unpackaged device showing its compactness. The TI-TENG comprises two distinct components that are divided by an air space: the vibrating part, which is vibrated by ultrasound waves, and the stationary part. In the vibrating part, ultrasound waves are transmitted through a liquid space with a thickness of 50 μm, confined between a Ti plate and a thin membrane. The gold

[1]Research and Development Center, Energymining Co., Ltd., Suwon 16226, Republic of Korea

[2]School of Advanced Materials Science and Engineering, Sungkyunkwan University, Suwon 16419, Republic of Korea

[3]Division Department of Materials Science and Engineering, Yonsei University, Seoul 03722, Republic of Korea

[4]Center for Human-Oriented Triboelectric Energy Harvesting, Yonsei University, Seoul 03722, Republic of Korea

[5]Department of Neurology, Samsung Medical Center, Sungkyunkwan University School of Medicine, Seoul 06351, Republic of Korea

[6]Cell and Gene Therapy Institute, Samsung Medical Center, Seoul 06351, Republic of Korea

[7]Samsung Advanced Institute for Health Sciences & Technology, Seoul 06351, Republic of Korea

[8]Department of Electronic Engineering, Gachon University, Seongnam 13120, Republic of Korea

[9]Department of Semiconductor Engineering, Gachon University, Seongnam 13120, Republic of Korea

[10]These authors contributed equally

[11]Lead contact

*Correspondence: kimagu@energymining.co.kr (H.-m.P.), yoonhj1222@gachon.ac.kr (H.-J.Y.), kimsw1@yonsei.ac.kr (S.-W.K.)

https://doi.org/10.1016/j.joule.2024.06.016

Please cite this article in press as: Chung et al., Gigantic triboelectric power generation overcoming acoustic energy barrier using metal-liquid coupling, Joule (2024), https://doi.org/10.1016/j.joule.2024.06.016

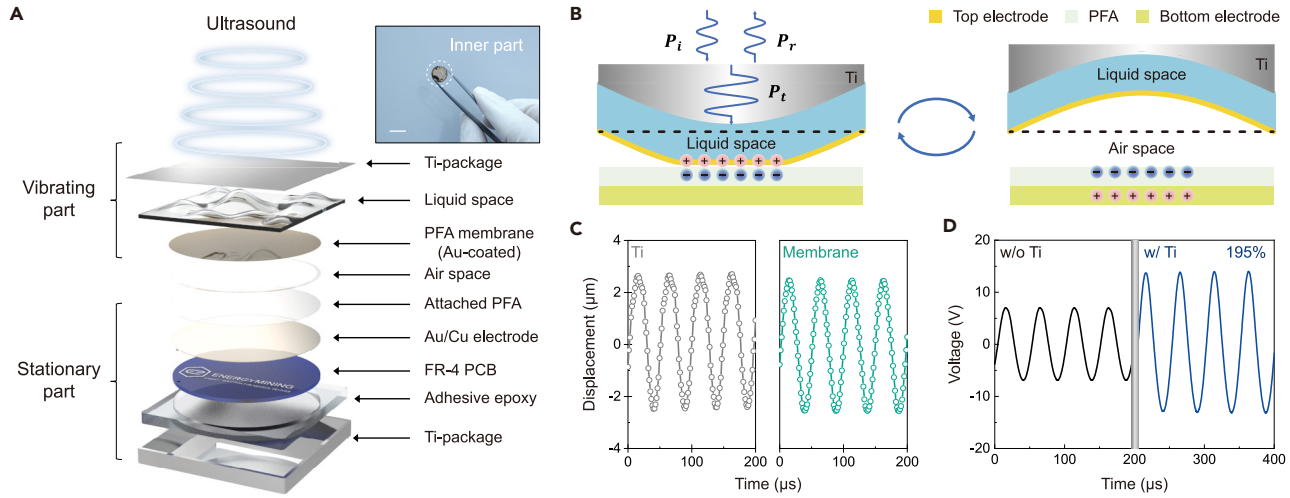

Figure 1. Design and working principle of the TI-TENG

(A) Exploded schematic illustration of the TI-TENG. The inset displays a photograph of the device, excluding the Ti packaging. Scale bars, 10 mm. See also Figures S1–S3.

(B) Schematic of the TI-TENG operation mechanism. P_i, P_r, and P_t denote incident, reflected, and transmitted pressure, respectively. See also Figure S4 and Note S1.

(C) Sinusoidal displacement amplitude of the Ti and membrane induced by 20 kHz ultrasound. See also Figure S6.

(D) Sinusoidal voltage output induced by 20 kHz ultrasound before and after applying Ti packaging on the TI-TENG. See also Figure S7.

(Au) layer on the surface of the membrane serves as both the top electrode and the contact material. In the stationary part, a perfluoroalkoxy (PFA) film with high tribo-negative properties is attached to the Au/copper (Cu) electrode deposited on the FR-4 printed circuit board (PCB), which is intended to contact the top electrode. An air space, with a thickness of 5 μm (Figure S1), is located between the two parts to provide space for contact electrification during membrane vibration,[24,25] while minimizing vibration in the stationary part.[26] The entire assembly is hermetically sealed with epoxy adhesive in order to fix each component inside the Ti packaging (Figures S2 and S3).

The TI-TENG operates in a double-electrode contact-separation mode[27] that is driven by 20 kHz ultrasound waves (Figure 1B). As ultrasound waves progress from soft tissue with a low acoustic impedance to Ti with a high acoustic impedance, the transmitted pressure on Ti is increased, as represented by Equation 1 for the transmitted coefficient of a normal incident plane wave:

$$T = \frac{2Z_2}{Z_2+Z_1} > 1 \rightarrow \frac{P_t}{P_i} > 1 \qquad \text{(Equation 1)}$$

where Z_n denotes the characteristic acoustic impedance for medium "n," and P_i and P_t denote the coefficient of the incident and transmitted pressure wave, respectively. When plane waves travel from medium 1 (soft tissue) to medium 2 (Ti), the transmitted coefficient is larger than 1, which means the transmitted pressure is larger than the incident pressure. This is due to the constructive interaction between the incident and reflected waves (details in Figure S4 and Note S1). The intense pressure generates elastic waves in Ti that are propagated to the membrane through the liquid space. The compressibility difference between the liquid and air space facilitates the vibration of the membrane. The incompressible fluid within the liquid space propagates the elastic waves from the Ti, whereas the compressible air space enables the membrane to vibrate. When the membrane vibrates, the triboelectric phenomenon arises between the top electrode and PFA, leading to negative charges

Please cite this article in press as: Chung et al., Gigantic triboelectric power generation overcoming acoustic energy barrier using metal-liquid coupling, Joule (2024), https://doi.org/10.1016/j.joule.2024.06.016

moving toward the inner surface of the PFA (2.16 nC cm^{-2}, Figure S5). As the membrane separates, the electrical potential of the top electrode increases relative to the bottom electrode, releasing the holes and resulting in a current that flows from the top to the bottom electrode. After the top electrode makes contact again, the electrical potential decreases, creating a reverse current. The ultrasound waves repeatedly induce the contact-separation process, thereby resulting in the formation of a current waveform with a frequency of 20 kHz.

The hypothesis proposing the coupling of Ti vibrations to those of the membrane is verified through laser vibrometer measurements (Figures 1C and S6). We measured the displacement of the Ti and the membrane under ultrasound irradiation, which revealed that both vibrate at 20 kHz with comparable magnitudes. In contrast to the inductive coupling, which results in a significant decline in the voltage output when enclosed in Ti packaging (Figure S7), the TI-TENG exhibited output amplification within the Ti packaging. It generates a voltage output of 195% relative to the non-Ti-TENG, as represented in Figure 1D.

Output amplification achieved through vibration mode control

To understand the physics behind the enhanced output generated by the TI-TENG in comparison to the non-Ti-TENG, we performed simulation and experimental analyses. The finite element method (FEM) computes the displacement of the vibration parts under different conditions. When a 20 kHz ultrasound travels to the non-Ti-TENG, the membrane vibrates in a multimode, generating multiple nodes and antinodes moving up and down (Figure 2A), consistent with the prior research.[5] By contrast, Ti vibrates in a single mode instead of the multimode (Figures 2B and 2C). The unimodal vibration mode is likely attributed to the relatively large mass and stiffness of a Ti plate compared with a polymeric membrane (Note S2). While the thickness of the Ti plate determines the vibration mode and displacement (Figure S8), we utilized Ti plates with a 0.5 mm thickness, the standard for commercial IMDs, in this research.[28] The air space between the Ti plate and the membrane acts as a barrier, inhibiting the transmission of elastic waves. Conversely, the liquid space facilitates the transmission of the elastic wave from the Ti plate to the membrane, thereby inducing unimodal oscillation in the membrane (Figures 2C and S9). When the generation of the elastic wave in the Ti by ultrasound waves is prevented, the membrane exhibits minimal vibration (Figure S10). Our finding supports the idea that the vibration of the Ti plate is indeed coupled with that of the membrane.

US-TENGs rely on the vibration of the membrane, giving rise to variations in mechanisms based on the vibration modes. Figures 2D and 2E illustrate the simplified working mechanism[29–31] based on the vibration modes: the multimode (Figure 2D) and the single mode (Figure 2E). In the multimode, both upward and downward-moving antinodes are present. The downward-moving antinodes decrease the electrical potential of the top electrode, whereas the upward-moving antinodes increase it. This offsetting action results in a reduction of the induced current. Conversely, in the single mode, the antinode is unidirectional, and there is no offsetting electrical potential. Figure S11 represents detailed electrical potential graphs for each case. As a result, it is apparent that US-TENGs generate enhanced electrical output when operated in a single mode (Note S3). We measured the open-circuit voltage (V_{OC}) and short-circuit current (I_{SC}) output of each device under 20 kHz ultrasound at the intensity of 430 mW cm^{-2} (Figures 2F and S12). Compared with the non-Ti-TENG, the device with Ti packaging generated a decreased output when combined with the air space, while the output increased when combined with the liquid space. We analyzed the average displacement data obtained from the FEM simulation and compared it to the device output (Figure 2G). The results reveal that the average

Please cite this article in press as: Chung et al., Gigantic triboelectric power generation overcoming acoustic energy barrier using metal-liquid coupling, Joule (2024), https://doi.org/10.1016/j.joule.2024.06.016

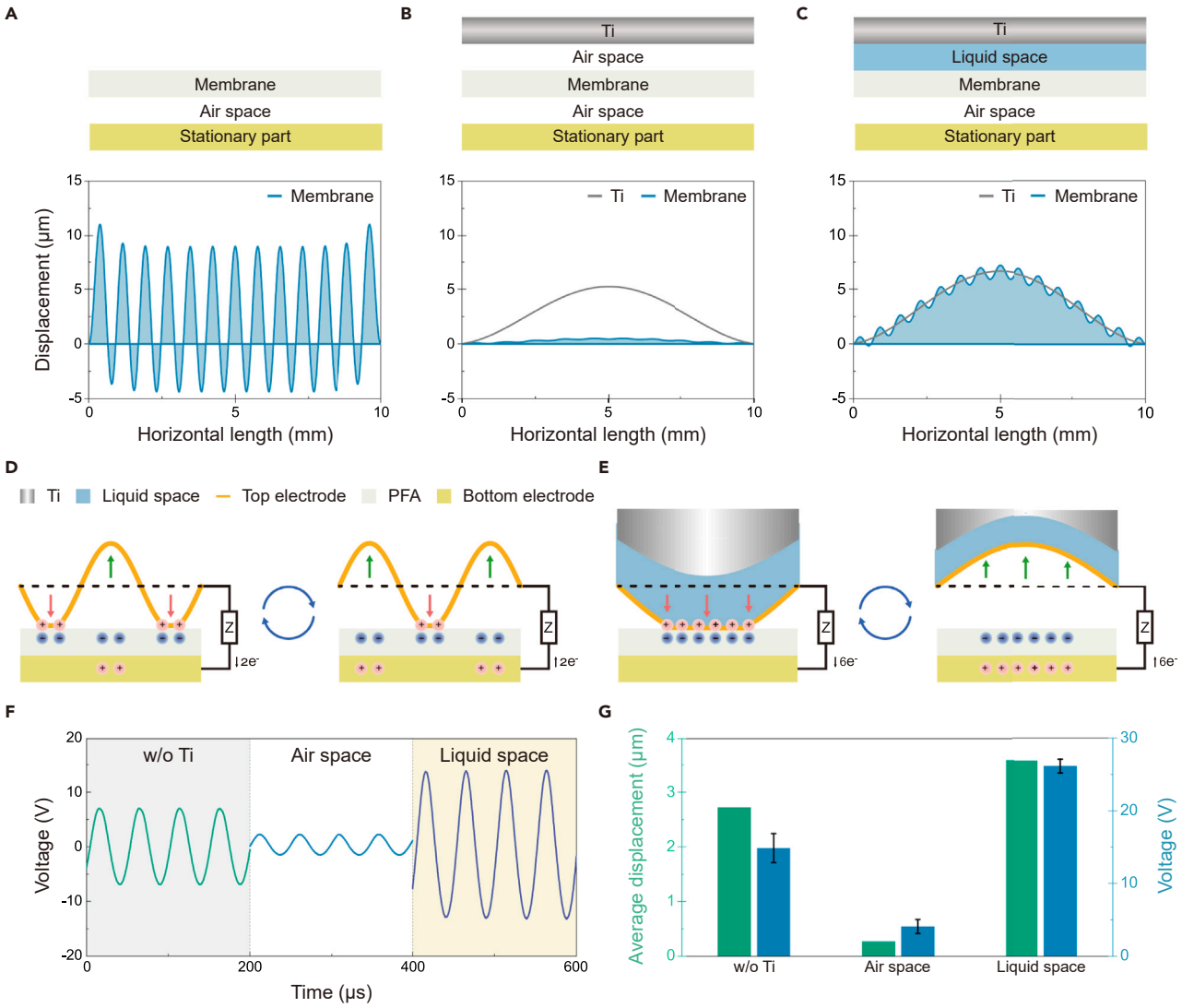

Figure 2. Output amplification achieved through vibration mode control

(A–C) Displacement data of the vibrating parts obtained by finite element method (FEM) simulation: without Ti (A), with Ti coupled with air space (B), and with Ti coupled with liquid space (C). See also Figures S8–S10 and Note S2.

(D and E) The simplified mechanism based on the vibration modes of the membrane including multimode (D) and single mode (E). See also Figure S11 and Note S3.

(F) Sinusoidal voltage outputs by different vibration part components. See also Figure S12.

(G) Comparison of average displacement data and voltage outputs. The voltage data (n = 5 for each group) are presented as mean values ± SD (standard deviation).

displacement trend closely follows the device output trend, supporting the correlation between vibration modes and the device output. We further compared the voltage output of the TI-TENG with that of the non-Ti-TENG at varying frequencies (Figure S13). Despite some variability, the amplification effect is present across a range of frequencies, thereby confirming the possibility of power transfer across various bandwidths.

Characterization of liquid materials for elastic wave propagation

Air hinders the transmission of elastic waves from Ti. In an ideal state without any air space between the Ti and membrane, the elastic wave can effectively progress from

Please cite this article in press as: Chung et al., Gigantic triboelectric power generation overcoming acoustic energy barrier using metal-liquid coupling, Joule (2024), https://doi.org/10.1016/j.joule.2024.06.016

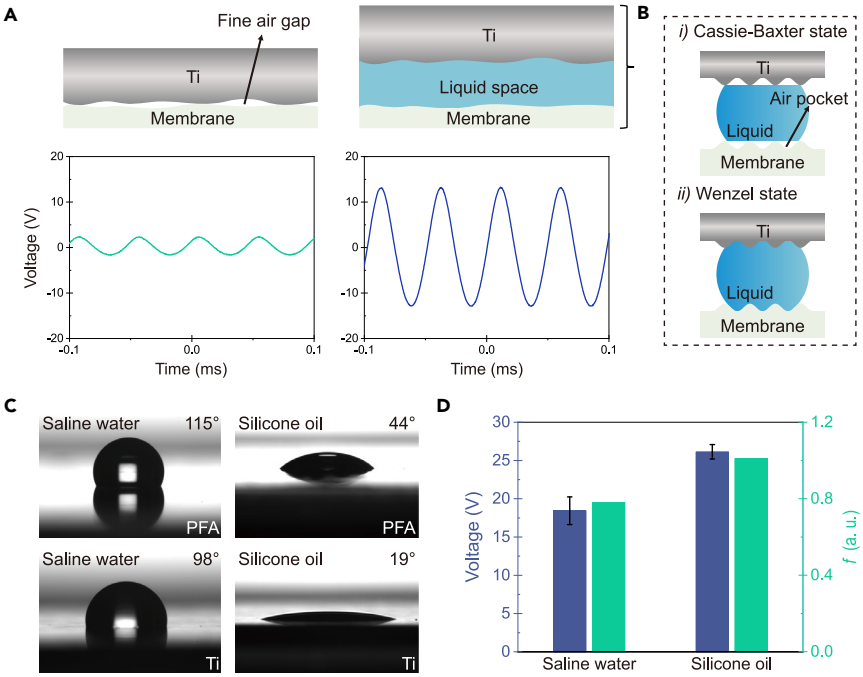

Figure 3. Characterization of liquid materials for elastic wave propagation

(A) 2D schematic illustrations and voltage outputs with and without liquid space. See also Figures S12 and S14.

(B) 2D schematic illustrations showing two ideal wetting states of the liquid space in solid interfaces.

(C) Contact angle image of each medical fluid at the interfaces of the Ti and PFA membrane.

(D) Voltage output (n = 5 for each group) and the calculated $r \cdot f$ value based on fluid type. The voltage data are presented as mean values ± SD. See also Figure S16 and Note S4.

the Ti plate to the membrane (Figure S14). Here, inevitable air pockets form between the Ti plate and the membrane in the dynamic state when ultrasound irradiates, resulting in lower ultrasound energy reaching the membrane (Figure 3A). In this regard, the role of the liquid space is to alleviate the presence of the air pockets in the dynamic state. To minimize the air pockets at solid interfaces, it is important to consider the wettability of the liquid space—the ability of a liquid to maintain contact with the solid surface.[32] Therefore, we compared two distinct liquids that are commercially available in the medical field: silicone oil and saline water.

At solid interfaces with microscopic roughness (Figure S15), liquid exists between two ideal wetting states: the Cassie-Baxter state and the Wenzel state (Figure 3B).[33–35] The Cassie-Baxter state is an incomplete wetting state where air pockets are entrapped at the solid-liquid interface, while the Wenzel state represents the complete wetting state where only liquids exist at the interface. To minimize the presence of air pockets at the solid interfaces in the vibrating part, the liquid space should closely exist in the Wenzel state. We characterized the wettability of the two medical liquids by measuring the contact angle (Figure 3C). The significantly lower contact angles at the interfaces indicate that silicone oil is more likely to be close to the Wenzel state when compared with saline water.

We further performed theoretical analysis using the Cassie-Baxter equation in a heterogeneous surface composed of air and solid surface as defined by Equation 2:[36]

$$\cos\theta_{real} = f_{solid}\cos\theta_{ideal} - f_{air} \quad \text{(Equation 2)}$$

In this equation, θ_{ideal} and θ_{real} represent Young's contact angle and measured contact angle, respectively. f denotes the proportion of the projected area of air or solid surface that is wet by a liquid. Since the total proportion is equal to 1, Equation 2 can be transformed into Equation 3:

$$\frac{\cos\theta_{real}+1}{\cos\theta_{ideal}+1} = f_{solid} \leq 1 \quad \text{(Equation 3)}$$

The wetting state is defined by calculating the f values of silicone oil and saline, with $f = 0$ representing the non-wetted Cassie-Baxter state and $f = 1$ approaching the fully wetted Wenzel state. Our investigation showed that the silicone oil is closer to the Wenzel state than saline water (Figure 3D; Tables S2 and S3; Note S4). Using silicone oil close to the Wenzel state led to an increase in V_{OC} output, which is consistent with our hypothesis. Since viscosity is the measure of a fluid's internal friction force,[37] we further compared the V_{OC} outputs of devices using silicone oil with varying viscosities. However, the result showed no discernible difference based on viscosity (Figure S16). We concluded that the mediation of the unimodal vibration mode within the liquid space is minimally affected by viscosity, and minimizing air pockets is an important factor for the TI-TENG performance.

Reliable output characterization under TMM

As the focus of this study is the development of a TET system for IMDs, it is essential to establish a standardized approach for the characterization of device output that takes into account the *in vivo* surroundings. Previous studies have conducted *ex vivo* output characterization using porcine tissue,[5,9] as it shares similarities with human anatomy. However, the *ex vivo* environment is subject to individual differences, which complicate the standardization. In this context, we propose a reproducible setup for characterizing TET performance using TMM (Figure 4A). It is a material that is recommended by International Electrotechnical Commision (IEC) International Standards[38] for evaluating the safety and efficacy of ultrasound equipment due to its comparable thermal and acoustic properties with those of human soft tissues. We fabricated the TMM according to the guidelines outlined in IEC 60601-2-37:2015 (Figure S17) and measured its density and sound speed to confirm its acoustic impedance similarity to human soft tissue. We found that the density of the fabricated TMM was 1,050 kg m^{-3}, the sound speed was 1,468 m s^{-1} (Figure S18), and the calculated acoustic impedance was 1,541 × 103 kg m^{-2} s^{-1}, indicating that it closely matches the acoustic impedance of soft human tissue (1,480 × 103 kg m^{-2} s^{-1}), as shown in Figure 4B.

Commercial rechargeable implantable pulse generators are usually implanted from around 20 to 25 mm depth.[39] Therefore, we characterized the output of the TI-TENG under TMM up to 30 mm to check the output according to the implantation depth (Figure 4C). The ultrasound's center frequency was configured at 20 kHz, with the intensity consistently maintained at 430 mW cm^{-2} (Figure S19). It is noteworthy that this intensity level is well below the safety standards established by the IEC and the United States Food and Drug Administration (FDA), ensuring compliance with human body safety regulations.[38,40] The practical thermal and mechanical stability of the ultrasound setup was demonstrated under the TMM and *in vivo* (Figures S20 and S21). At 5 mm depth, the TI-TENG generates V_{OC} peaks of 26.3 V. The voltage output slightly decreased with depth, but the output remained at 83% even at a depth of 30 mm, showing the potential for the TI-TENG to be implanted at a deep site in the body. Comparing the *in vivo* voltage output beneath

Please cite this article in press as: Chung et al., Gigantic triboelectric power generation overcoming acoustic energy barrier using metal-liquid coupling, Joule (2024), https://doi.org/10.1016/j.joule.2024.06.016

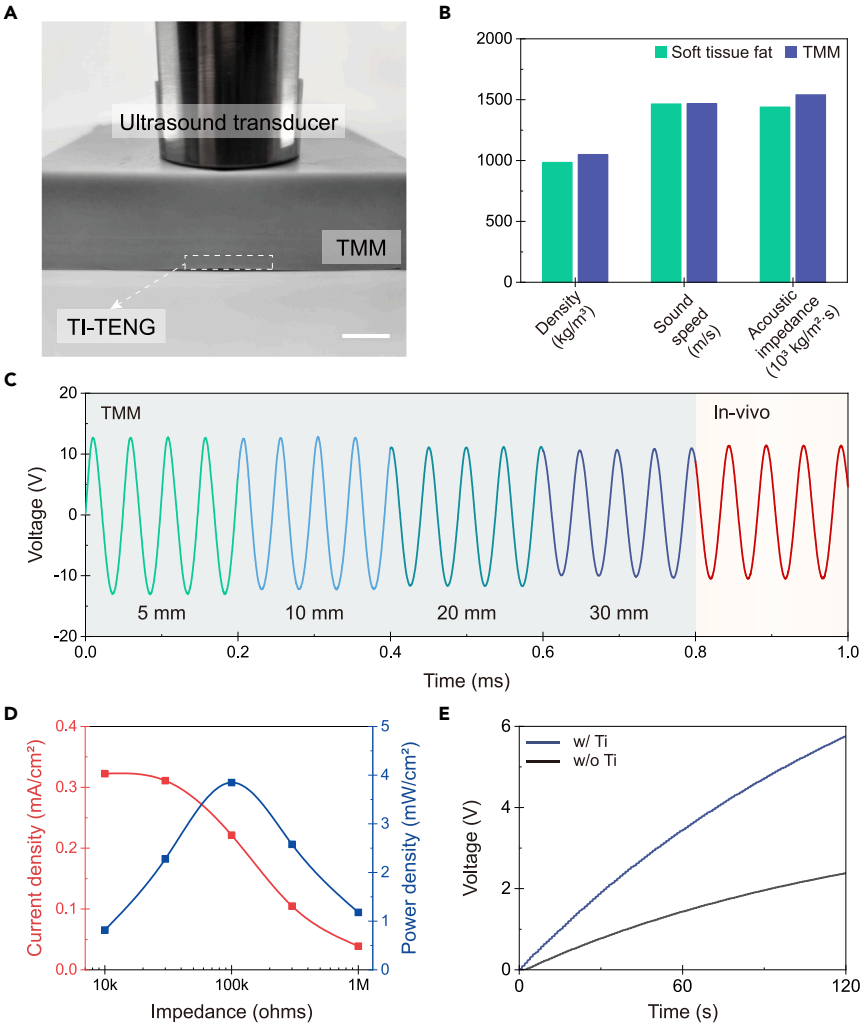

Figure 4. Reliable output characterization under TMM

(A) Experimental setup for output measurement of the TI-TENG using TMM. Scale bars, 10 mm. See also Figure S17.

(B) Comparison of acoustic properties of TMM with human soft tissue. See also Figure S18.

(C–E) Electrical characterization of TI-TENG induced by 20 kHz ultrasound. The voltage output obtained under TMM with different thicknesses and *in vivo* output obtained under the dorsum of a rat (C). Maximum current and power output depending on the electrical impedance under 20 mm TMM (D). Charging curve of a 1mF capacitor with the TI-TENG and the non-Ti-TENG (E). See also Figures S22–S24.

the skin on the dorsum of a rat (Figures 4C and S22) with the output under TMM, no significant deviation was observed. This suggests the potential for standardizing TMM-based output characterization. The slight difference in voltage outputs measured under TMM and *in vivo* at equivalent depths may be attributed to the dissimilarity between the human tissue emulated by TMM and that of rats.

We further characterized the optimal impedance and maximum power density of the device at a depth of 20 mm and found that it generates a power density of 3.85 mW cm^{-2} at 100 kΩ impedance (Figure 4D), which is 310% and 6,400% relative to the non-Ti-TENG and the Ti-packaged TENG without liquid, respectively (Figure S23). It is worth noting that the TI-TENG produces the highest power density compared

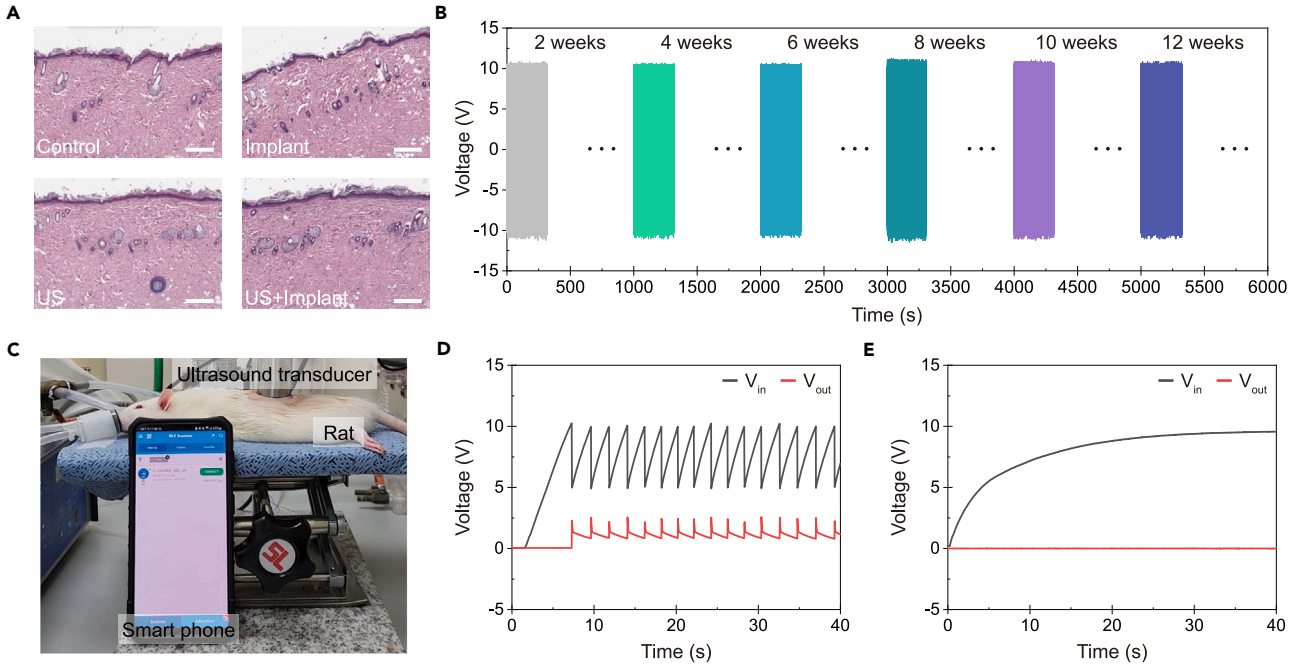

Figure 5. *In vivo* energy transfer using the TI-TENG

(A) H&E-stained subdermal tissue images in implanted parts. The term "implant" refers to the implantation of the TI-TENG, and the "US" indicates the irradiation of ultrasound on the implanted parts. Scale bars, 0.25 mm. See also Figure S26.

(B) Voltage output characterization during long-term *in vivo* operation.

(C) Experimental setup for *in vivo* Bluetooth operation using the TI-TENG. See also Figure S27.

(D and E) Charging and discharging graph of the PMIC during TI-TENG operation (D) and non-Ti-TENG operation (E).

with the previous US-TENGs (Table S1). In the context of power modulation circuit application, we analyzed capacitor-charging performance (Figure S24). The TI-TENG charged a 1 mF capacitor to 5.6 V within 2 min, a rate 2.4 times faster than the non-Ti-TENG (Figure 4E). This result suggests the significance of the technology for driving circuits in biomedical applications embedded within Ti packaging.

In vivo energy transfer using the TI-TENG

We evaluated the biocompatibility of the TI-TENG through the 3-*(1, 2)*-2,5-diphenyl-2, H-tetrazolium bromide (MTT) assay and comet assay. The results indicate that the TI-TENG is safe from cytotoxicity and genotoxicity (Figure S25). To check the inflammatory response of the proposed TET system, we implanted the device for a month and applied ultrasound for 10 min at 1-day intervals. The hematoxylin and eosin (H&E) staining on the subdermal tissue in the implanted part indicated that no inflammatory reactions were observed (Figures 5A and S26). To check the long-term stability, the device was implanted under the skin on the dorsum of a rat. We applied ultrasound to the implanted site and measured the output voltage biweekly. As shown in Figure 5B, it was found to generate a consistent output without any deterioration over 3 months. The remarkable stability of the TI-TENG is attributed to two primary impacts of the Ti packaging: it shields the internal assembly from exposure to biofluid during long-term implantation and supports the membrane in maintaining the simple vibration mode, thereby prolonging its longevity.

IMDs, which perform multiple functions inside the human body such as neurostimulation or physiological monitoring, require monitoring technology to ensure optimal

Please cite this article in press as: Chung et al., Gigantic triboelectric power generation overcoming acoustic energy barrier using metal-liquid coupling, Joule (2024), https://doi.org/10.1016/j.joule.2024.06.016

performance. Therefore, we demonstrated the practical application of TI-TENG by illustrating Bluetooth communication using our device (Figure 5C). The alternating current (AC) output from the TI-TENG was modulated by the power management integrated circuit (PMIC) to operate the Bluetooth module (Figure S27). The PMIC rectifies the AC output and charges its built-in capacitor to 10 V, which is then discharged to 5 V. The discharged power is converted into an output voltage of 2.5 V via a direct current (DC) to DC converter. Figure 5D shows the charging and discharging graph of the PMIC during TI-TENG operation. The TI-TENG continuously charged and discharged the capacitor and successfully operated the Bluetooth module within a few seconds (Figure 5C; Video S1). By contrast, the non-TI-TENG failed to charge the capacitor to 10 V, resulting in the inability to discharge the desired output voltage (Figure 5E). This highlights the enhanced energy transfer performance through the Ti packaging.

DISCUSSION

This work represents the first TET technology with enhanced performance, overcoming energy attenuation caused by Ti packaging. The Ti packaging has been serving as a barrier that obstructs the transmission of ultrasound, resulting in a decrease in power transfer efficiency. Moreover, the multimode vibration of the membrane in US-TENGs has been considered to offset the induced electrical potential, which also significantly decreases the efficiency. We addressed both challenges simultaneously through the novel structural design of TI-TENG. The considerable difference in acoustic impedance between a Ti plate and a soft tissue causes a substantial reflection of the ultrasound but also induces an intense pressure on the Ti plate, which in turn generates elastic waves within it. The elastic waves from the Ti plate are transmitted to the membrane through strategically arranged incompressible liquid and compressible air spaces. We verified through experiments and simulations that the higher electrical potential difference resulting from the unidirectional vibration of the membrane leads to a significant increase in power output compared with the design without Ti packaging. Our study of the liquid space material revealed that wetting properties play a critical role in minimizing air pockets, which otherwise impede the transmission of vibrations from the Ti plate. We characterized the electrical performance of the optimized TI-TENG using bio-safe ultrasound in a TMM environment that simulates human tissue and verified its practical usability *in vivo*. Bluetooth communication was successfully implemented with the assistance of the Ti packaging, highlighting the technology's significance.

IMDs are evolving to perform more functions with a smaller size and longer lifespan.[13] The Ti packaging in IMDs serves the contradictory role of protecting internal components while also impeding energy transfer. Replacement of the Ti packaging remains impractical due to the inherent characteristics of IMDs, encompassing considerable implantation expenses and prolonged implantation inside the human body. Therefore, a TET technology capable of employing smaller receivers and delivering energy via Ti packaging with high efficiency is poised to match the progress of IMDs. In this regard, current technologies fall short of the requirements. Our work presents a miniaturized TET system wherein the presence of Ti packaging enhances energy transfer efficiency. Advanced structure designs to guide or focus ultrasound waves onto a device and comprehensive investigations into the material and structure of TENGs will further enhance its capabilities. We foresee this technology playing a crucial role in advancing the next generation of IMDs.

Please cite this article in press as: Chung et al., Gigantic triboelectric power generation overcoming acoustic energy barrier using metal-liquid coupling, Joule (2024), https://doi.org/10.1016/j.joule.2024.06.016

CellPress

EXPERIMENTAL PROCEDURES

Resource availability

Lead contact

Further information and requests for resources should be directed to and will be fulfilled by the lead contact, Sang-Woo Kim (kimsw1@yonsei.ac.kr).

Materials availability

This study did not generate new, unique materials.

Data and code availability

The datasets generated during this study are available from the lead contact upon reasonable request.

Fabrication of materials and devices

Device fabrication

The device fabrication process is described in Figure S2. The device consisted of a PCB substrate whose FR-4 glass epoxy layer was covered by Cu and Au, conductive carbon tape, PFA membrane, polydimethylsiloxane (PDMS) spacer, Au-coated PFA membrane, and epoxy. Conductive carbon tape from Sunghosigma was attached to the PCB substrate. A 25 μm thick PFA membrane from ALPHAFLON was attached to the conductive carbon tape. PDMS was spin-coated for 300 s at 4,000 rpm on PFA to form a 5 μm space gap at the edge of the PFA membrane. Au-coated PFA membrane was placed on the PDMS spacer and sealed using epoxy (EPO-TEK 301).

Ti integration

The Ti integration process is described in Figure S3. Masking tape (50 μm) was attached to the center of a Ti plate to create space for the liquid. Then, a 50 μm thick layer of epoxy (EPO-TEK 301) was applied as a spacer using an automatic bar coater. After the epoxy was cured, the masking tape was removed from the Ti plate. Then, liquid was applied within the epoxy spacer using blade coating. The TENG device was positioned on the Ti plate and sealed with epoxy (EPO-TEK 301). Following a second curing process, the Ti plate was attached to a Ti body.

TMM fabrication

The TMM fabrication process is described in Figure S17. Prepare and mix the constituent substances in a flask according to the weight ratio specified in the recipe presented in the standards IEC 60601-2-5 and IEC 60601-2-37. The mixed solution was degassed using a vacuum pump while stirring for 1 h and stirred in a 95°*C* water bath for 30 min. After cooling to 47°*C*, the solution was poured into the mold.

Characterizations

Material and device characterization

To measure the surface roughness of the Ti plate and the PFA membrane, topography measurement was conducted using HITACHI AFM5000II, and a 10 × 10 μm size area was scanned at a rate of 0.3 Hz. To characterize the air spacer between the PFA membrane and the PCB, field emission scanning electron microscopy (FE-SEM) and energy dispersive X-ray spectroscopy (EDS) measurements were performed using HITACHI SU 5000.

Laser vibrometer measurement

The displacement amplitudes of the Ti and membrane in the TI-TENG were measured using a laser vibrometer (Polytec PSV-500). Since the laser vibrometer uses the reflection of light, modified devices were fabricated to measure the

Please cite this article in press as: Chung et al., Gigantic triboelectric power generation overcoming acoustic energy barrier using metal-liquid coupling, Joule (2024), https://doi.org/10.1016/j.joule.2024.06.016

displacement of the Ti and the membrane, respectively. For the Ti displacement measurement, a device with no electrodes under the Ti was fabricated. A bare membrane was used without the top electrode, and the bottom substrate was replaced by a glass substrate. The Ti was irradiated with ultrasound, and the lower part was irradiated with a laser to measure the displacement. To measure the displacement of the membrane, a modified device was made by coating a top electrode on the membrane in the above structure, and the displacement was measured in the same way.

Simulation

FEM simulations were performed using COMSOL Multiphysics. Physical parameters about aluminum (Al) and air were taken from the library in COMSOL Multiphysics. We used the common reference data for Ti, PFA, silicone oil, and fat tissue. We added an ultrasound probe load with a 3 cm diameter and a pressure of 1×10^5 Pa. The TI-TENG was placed inside the fat tissue and centered under the ultrasound probe. We run pressure acoustics, solid mechanics, and acoustic-structure physics to simulate ultrasound at 20 kHz, its acoustic and mechanic interaction with device parts, and the movement of the membrane. The mechanical contact between the membrane and the electrode was not taken into account during FEM simulations. For comparison purposes, the calculations were performed with various dimensions and materials for Ti and the liquid space.

Electrical characterization

Voltage signals were measured and recorded using an oscilloscope (Keysight MSOX3054T) with a voltage probe (Keysight N2843A) with 10 MΩ input impedance. The voltages for the capacitors were measured using a digital multimeter (Keysight 34470A). Current signals were measured using a low-noise current preamplifier (Stanford Research Systems SR570) with an input impedance of 1 Ω. Ultrasound generation and characterization were carried out using a commercial ultrasound transducer and generator (Mirae MV100). The power of ultrasound was measured using an ultrasound power meter (Ohmic instruments UPM-DT-1), and the intensity of ultrasound was calculated by dividing the ultrasound power by the transducer area. The charge output was measured using an electrometer (Keithley 6514).

MTT assay and comet assay

To perform the MTT assay, human fibroblasts (ATCC, CRL–1502; designation: WS1; product category: human cells; organism: *Homo sapiens*, human; cell type: fibroblast; morphology: fibroblast) and culture medium were added after placing experimental materials into each well of 96-well plates (10,000 cells per well, final volume: 100 μL). Then, we incubated the fibroblasts for periods of 24, 48, and 72 h. Subsequently, we removed the culture medium from the 96-well plates and added 50 μL of serum-free medium and 50 μL of MTT solution (Abcam, 5 mg mL^{-1}) into each well. The plate was incubated at 37°C for 2 h. Then, we removed the serum-free medium and the MTT solution. We cleaned the samples by rinsing them with diluted phosphate-buffered saline (PBS) solution and added 150 μL of a solubilizing agent (dimethyl sulfoxide, Sigma-Aldrich) to dissolve the formazan crystals for 15 min. Finally, we transferred 100 μL of the solution to another 96-well plate and measured the absorbance at optical density (OD) = 590 nm.

To perform the comet assay, we first prepared a lysis buffer (Thermo Fisher Scientific), alkaline solution (SAMCHUN chemical), and tris-borate ethylene-diamine-tetra-acetic acid (TBE) electrophoresis solution (Thermo Fisher Scientific). We melted the agarose gel until it was liquefied and added 75 μL of the agarose gel to the slide to

Please cite this article in press as: Chung et al., Gigantic triboelectric power generation overcoming acoustic energy barrier using metal-liquid coupling, Joule (2024), https://doi.org/10.1016/j.joule.2024.06.016

CellPress

form the base layer. Then, we kept the slide at 4°C for 15 min. Human fibroblasts were mixed with agarose gel in a 1:10 ratio, and 75 μL of this mixture was transferred on top of the base layer. The slide was again kept at 4°C for 15 min. The slide was then sequentially immersed in pre-chilled lysis buffer (25 mL) for 60 min, alkaline solution (25 mL) for 30 min at 4°C in dark conditions, and TBE electrophoresis solution for 10 min, maintaining the temperature and darkness as required. For electrophoresis, the chamber was filled with cold TBE electrophoresis solution until the slides were covered, and an electric field of 0.1 V mm^{-1} was applied for 15 min. After electrophoresis, the slide was rinsed three times with pre-chilled deionized water and a 70% ethanol solution. Once dry, 100 μL of diluted Vista Green DNA dye was added to the slide, and it was incubated for 15 min at room temperature. Finally, we observed the slide using epifluorescence microscopy with a fluorescein isothiocyanate (FITC) filter and measured the olive tail moment (OTM).

In vivo *wireless energy transmission*

For *in vivo* electrical characterization, we induced anesthesia in an 8-week-old Sparague-Dawley rat model through inhalation of isoflurane from Hana Pharm Co., Ltd. Subsequently, the rat was positioned prone, and its back was shaved. A povidone-iodine prep pad from Green Pharm Co., Ltd. was topically applied on shaved skin. After UV sterilization, the TI-TENG was implanted beneath the dermis, and the incisions were closed using skin sutures. The surgical site was covered with sterilized gauze, and the rat was allowed a 3-day recovery period for both the surgical wound and the biological integration of the TI-TENG. Then, anesthesia was conducted on the rat, and ultrasound was applied to the rat at a 5 mm distance from the probe. A PMIC (LTC3331) from Linear Technology, Inc. was used to convert the AC TENG output into a DC output of 2.5 V. The rectified power output was used to operate a customized Bluetooth module. Throughout this process, the rat was placed under an infrared heater to maintain its body temperature. All studies on rats were approved by the Institutional Animal Care and Use Committee (IACUC) of Samsung Medical Center (20230421001).

SUPPLEMENTAL INFORMATION

Supplemental information can be found online at https://doi.org/10.1016/j.joule.2024.06.016.

ACKNOWLEDGMENTS

This work was financially supported by the Bio & Medical Technology Development Program (2022M3E5E9016662) and the Basic Science Research Program (2022R1A3B1078291) through the National Research Foundation of Korea (NRF), funded by the Ministry of Science and ICT (MSIT, Korea); the Entrepreneurship Development Program (S3282292), funded by the Ministry of SMEs and Startups (MSS, Korea); and the Next Generation Intelligence Semiconductor Foundation Program (20025736), funded by the Ministry of Trade, Industry & Energy (MOTIE, Korea).

AUTHOR CONTRIBUTIONS

Conceptualization, Y.C., J.-M.J., J.-H.H., and S.-W.K.; methodology, Y.C., J.-M.J., J.-H.H., and Y.-J.K.; investigation, Y.C., J.-M.J., J.-H.H., Y.-J.K., B.-J.P., D.S.C., and H.-M.P.; visualization, Y.C., J.-M.J., and J.-H.H.; funding acquisition, H.-M.P. and S.-W.K.; project administration, Y.C., J.-M.J., H.-J.Y., and S.-W.K.; supervision, H.-J.Y. and S.-W.K.; writing – original draft, Y.C., J.-M.J., and J.-H.H.; writing – review & editing, Y.C., H.-M.P., H.-J.Y., and S.-W.K.

DECLARATION OF INTERESTS

Y.C., J.-M.J., J.-H.H., and H.-M.P. are inventors on a patent (KR 10–2620483) granted through Energymining Co., Ltd. that covers the use of a liquid matching layer to enhance the electrical output of titanium-packaged ultrasound-driven triboelectric nanogenerator.

Received: March 31, 2024
Revised: May 13, 2024
Accepted: June 19, 2024
Published: July 16, 2024

REFERENCES

1. Madhvapathy, S.R., Wang, J.-J., Wang, H., Patel, M., Chang, A., Zheng, X., Huang, Y., Zhang, Z.J., Gallon, L., and Rogers, J.A. (2023). Implantable bioelectronic systems for early detection of kidney transplant rejection. Science *381*, 1105–1112. https://doi.org/10.1126/science.adh7726.

2. Mickle, A.D., Won, S.M., Noh, K.N., Yoon, J., Meacham, K.W., Xue, Y., McIlvried, L.A., Copits, B.A., Samineni, V.K., Crawford, K.E., et al. (2019). A wireless closed-loop system for optogenetic peripheral neuromodulation. Nature *565*, 361–365. https://doi.org/10.1038/s41586-018-0823-6.

3. Ho, J.S., Yeh, A.J., Neofytou, E., Kim, S., Tanabe, Y., Patlolla, B., Beygui, R.E., and Poon, A.S.Y. (2014). Wireless power transfer to deep-tissue microimplants. Proc. Natl. Acad. Sci. USA *111*, 7974–7979. https://doi.org/10.1073/pnas.1403002111.

4. Won, S.M., Cai, L., Gutruf, P., and Rogers, J.A. (2023). Wireless and battery-free technologies for neuroengineering. Nat. Biomed. Eng. *7*, 405–423. https://doi.org/10.1038/s41551-021-00683-3.

5. Hinchet, R., Yoon, H.-J., Ryu, H., Kim, M.-K., Choi, E.-K., Kim, D.-S., and Kim, S.-W. (2019). Transcutaneous ultrasound energy harvesting using capacitive triboelectric technology. Science *365*, 491–494. https://doi.org/10.1126/science.aan3997.

6. Meng, X., Xiao, X., Jeon, S., Kim, D., Park, B.J., Kim, Y.J., Rubab, N., Kim, S., and Kim, S.W. (2023). An ultrasound-driven bioadhesive triboelectric nanogenerator for instant wound sealing and electrically accelerated healing in emergencies. Adv. Mater. *35*, e2209054. https://doi.org/10.1002/adma.202209054.

7. Lee, D.-M., Kang, M., Hyun, I., Park, B.-J., Kim, H.J., Nam, S.H., Yoon, H.-J., Ryu, H., Park, H.-M., Choi, B.-O., and Kim, S.W. (2023). An on-demand bioresorbable neurostimulator. Nat. Commun. *14*, 7315. https://doi.org/10.1038/s41467-023-42791-5.

8. Liu, X., Wang, Y., Wang, G., Ma, Y., Zheng, Z., Fan, K., Liu, J., Zhou, B., Wang, G., You, Z., et al. (2022). An ultrasound-driven implantable wireless energy harvesting system using a triboelectric transducer. Matter *5*, 4315–4331. https://doi.org/10.1016/j.matt.2022.08.016.

9. Lee, D.-M., Rubab, N., Hyun, I., Kang, W., Kim, Y.-J., Kang, M., Choi, B.O., and Kim, S.-W. (2022). Ultrasound-mediated triboelectric nanogenerator for powering on-demand transient electronics. Sci. Adv. *8*, eabl8423. https://doi.org/10.1126/sciadv.abl8423.

10. Liu, W., Wang, Z., Wang, G., Liu, G., Chen, J., Pu, X., Xi, Y., Wang, X., Guo, H., Hu, C., Wang, Z.L., et al. (2019). Integrated charge excitation triboelectric nanogenerator. Nat. Commun. *10*, 1426. https://doi.org/10.1038/s41467-019-09464-8.

11. Zhou, L., Liu, D., Zhao, Z., Li, S., Liu, Y., Liu, L., Gao, Y., Wang, Z.L., and Wang, J. (2020). Simultaneously enhancing power density and durability of sliding mode triboelectric nanogenerator via interface liquid lubrication. Adv. Energy Mater. *10*, 2002920. https://doi.org/10.1002/aenm.202002920.

12. Yoon, H.-J., and Kim, S.-W. (2020). Nanogenerators to power implantable medical systems. Joule *4*, 1398–1407. https://doi.org/10.1016/j.joule.2020.05.003.

13. Nair, V., Dalrymple, A.N., Yu, Z., Balakrishnan, G., Bettinger, C.J., Weber, D.J., Yang, K., and Robinson, J.T. (2023). Miniature battery-free bioelectronics. Science *382*, eabn4732. https://doi.org/10.1126/science.abn4732.

14. Joung, Y.-H. (2013). Development of implantable medical devices: from an engineering perspective. Int. Neurourol. J. *17*, 98–106. https://doi.org/10.5213/inj.2013.17.3.98.

15. Teo, A.J.T., Mishra, A., Park, I., Kim, Y.-J., Park, W.-T., and Yoon, Y.-J. (2016). Polymeric biomaterials for medical implants and devices. ACS Biomater. Sci. Eng. *2*, 454–472. https://doi.org/10.1021/acsbiomaterials.5b00429.

16. Zhang, S., Zhou, Y., Libanori, A., Deng, Y., Liu, M., Zhou, M., Qu, H., Zhao, X., Zheng, P., Zhu, Y.-L., et al. (2023). Biomimetic spinning of soft functional fibres via spontaneous phase separation. Nat. Electron. *6*, 338–348. https://doi.org/10.1038/s41928-023-00960-w.

17. Zhang, S., Deng, Y., Libanori, A., Zhou, Y., Yang, J., Tat, T., Yang, L., Sun, W., Zheng, P., Zhu, Y.L., et al. (2023). In situ grown silver–polymer framework with coordination complexes for functional artificial tissues. Adv. Mater. *35*, e2207916. https://doi.org/10.1002/adma.202207916.

18. Culjat, M.O., Choi, M., Singh, R.S., Grundfest, W.S., Brown, E.R., and White, S.N. (2008). Ultrasound detection of submerged dental implants through soft tissue in a porcine model. J. Prosthet. Dent. *99*, 218–224. https://doi.org/10.1016/S0022-3913(08)60046-3.

19. Kim, Y.-J., Lee, J., Hwang, J.-H., Chung, Y., Park, B.-J., Kim, J., Kim, S.-H., Mun, J., Yoon, H.-J., Park, S.-M., et al. (2024). High-performing and capacitive-matched triboelectric implants driven by ultrasound. Adv. Mater. *36*, e2307194. https://doi.org/10.1002/adma.202307194.

20. Lee, T.-G., Jo, S.-H., Seung, H.M., Kim, S.-W., Kim, E.-J., Youn, B.D., Nahm, S., and Kim, M. (2020). Enhanced energy transfer and conversion for high performance phononic crystal-assisted elastic wave energy harvesting. Nano Energy *78*, 105226. https://doi.org/10.1016/j.nanoen.2020.105226.

21. Allam, A., Sabra, K., and Erturk, A. (2021). Sound energy harvesting by leveraging a 3D-printed phononic crystal lens. Appl. Phys. Lett. *118*, 103504. https://doi.org/10.1063/5.0030698.

22. Chen, C., Wen, Z., Shi, J., Jian, X., Li, P., Yeow, J.T.W., and Sun, X. (2020). Micro triboelectric ultrasonic device for acoustic energy transfer and signal communication. Nat. Commun. *11*, 4143. https://doi.org/10.1038/s41467-020-17842-w.

23. Deng, W., Libanori, A., Xiao, X., Fang, J., Zhao, X., Zhou, Y., Chen, G., Li, S., and Chen, J. (2022). Computational investigation of ultrasound induced electricity generation via a triboelectric nanogenerator. Nano Energy *91*, 106656. https://doi.org/10.1016/j.nanoen.2021.106656.

24. Niu, S., Wang, S., Lin, L., Liu, Y., Zhou, Y.S., Hu, Y., and Wang, Z.L. (2013). Theoretical study of contact-mode triboelectric nanogenerators as an effective power source. Energy Environ. Sci. *6*, 3576–3583. https://doi.org/10.1039/C3EE42571A.

25. Zhang, Q., Liang, Q., Nandakumar, D.K., Qu, H., Shi, Q., Alzakia, F.I., Tay, D.J.J., Yang, L., Zhang, X., Suresh, L., et al. (2021). Shadow enhanced self-charging power system for wave and solar energy harvesting from the ocean. Nat. Commun. *12*, 616. https://doi.org/10.1038/s41467-021-20919-9.

26. Powles, A.E., Martin, D.J., Wells, I.T., and Goodwin, C.R. (2018). Physics of ultrasound. Anaesth. Intensive Care Med. *19*, 202–205. https://doi.org/10.1016/j.mpaic.2018.01.005.

Please cite this article in press as: Chung et al., Gigantic triboelectric power generation overcoming acoustic energy barrier using metal-liquid coupling, Joule (2024), https://doi.org/10.1016/j.joule.2024.06.016

27. Bai, Y., Feng, H., and Li, Z. (2022). Theory and applications of high-voltage triboelectric nanogenerators. Physical Science *3*, 101108. https://doi.org/10.1016/j.xcrp.2022.101108.

28. Radziemski, L., and Makin, I.R.S. (2016). In vivo demonstration of ultrasound power delivery to charge implanted medical devices via acute and survival porcine studies. Ultrasonics *64*, 1–9. https://doi.org/10.1016/j.ultras.2015.07.012.

29. Lone, S.A., Lim, K.C., Kaswan, K., Chatterjee, S., Fan, K.-P., Choi, D., Lee, S., Zhang, H., Cheng, J., and Lin, Z.-H. (2022). Recent advancements for improving the performance of triboelectric nanogenerator devices. Nano Energy *99*, 107318. https://doi.org/10.1016/j.nanoen.2022.107318.

30. Yeh, C., Kao, F.-C., Wei, P.-H., Pal, A., Kaswan, K., Huang, Y.-T., Parashar, P., Yeh, H.-Y., Wang, T.-W., Tiwari, N., et al. (2022). Bioinspired shark skin-based liquid metal triboelectric nanogenerator for self-powered gait analysis and long-term rehabilitation monitoring. Nano Energy *104*, 107852. https://doi.org/10.1016/j.nanoen.2022.107852.

31. Lin, Z.-H., Cheng, G., Lin, L., Lee, S., and Wang, Z.L. (2013). Water-solid surface contact electrification and its use for harvesting liquid-wave energy. Angew. Chem. Int. Ed. Engl. *52*, 12545–12549. https://doi.org/10.1002/anie.201307249.

32. Zhang, P., Wang, S., Wang, S., and Jiang, L. (2015). Superwetting surfaces under different media: effects of surface topography on wettability. Small *11*, 1939–1946. https://doi.org/10.1002/smll.201401869.

33. Wenzel, R.N. (1936). Resistance of solid surfaces to wetting by water. Ind. Eng. Chem. *28*, 988–994. https://doi.org/10.1021/ie50320a024.

34. Cassie, A.B.D., and Baxter, S. (1945). Large contact angles of plant and animal surfaces. Nature *155*, 21–22. https://doi.org/10.1038/155021a0.

35. Nagayama, G., and Zhang, D. (2020). Intermediate wetting state at nano/microstructured surfaces. Soft Matter *16*, 3514–3521. https://doi.org/10.1039/C9SM02513H.

36. Shim, M.H., Kim, J., and Park, C.H. (2014). The effects of surface energy and roughness on the hydrophobicity of woven fabrics. Text. Res. J. *84*, 1268–1278. https://doi.org/10.1177/0040517513495945.

37. Mizerovskiy, L.N., and Smirnov, P.R. (2021). Viscosity and internal friction in liquids. Russ. J. Gen. Chem. *91*, 1797–1806. https://doi.org/10.1134/S1070363221090279.

38. Monteiro Souza, R., de Assis, M.K.M., Pereira Barretto da Costa-Félix, R., and Victor Alvarenga, A. (2022). Speed of sound in the IEC tissue-mimicking material and its maintenance solution as a function of temperature. Ultrasonics *118*, 106564. https://doi.org/10.1016/j.ultras.2021.106564.

39. Pritzlaff, S.G., and Fishman, S.M. (2023). Spinal Cord Stimulation: Percutaneous Implantation Techniques (Oxford University Press).

40. Moreno-Gomez, N., Athanassiadis, A.G., Poortinga, A.T., and Fischer, P. (2023). Antibubbles enable tunable payload release with low-intensity ultrasound. Adv. Mater. *35*, e2305296. https://doi.org/10.1002/adma.202305296.